

Low RCS Multi-Bit Coding Metasurface Modeling and Optimization: MoM-GEC Method in Conjunction with Genetic Algorithm

Imen Soltani*, Takoua Soltani, and Taoufik Aguil

Abstract—We propose a new approach to design multi-bit coding metasurfaces (MSs) for broadband terahertz scattering reduction. An anisotropic graphene-based element with multiple reflection phase responses is modeled using the Method of Moments combined with the Generalized Equivalent Circuit's approach (MoM-GEC). The multi-level reflection phase response is adjusted by tuning the graphene chemical potential of each cell. Based on the coding metamaterials concept, 1-bit MS building blocks are nominated as “0” and “1” elements with opposite phase responses 0° and 180° , respectively. Therefore, the genetic algorithm (GA) is employed to search the optimal reflection phase matrix and determine the best coding metasurface layout. In order to validate our design strategy, 4×4 , 8×8 , 16×16 , 32×32 , and 64×64 arrays (MS) are modeled and show a great agreement with the desired low Radar Cross Section (RCS). In addition, 2-bit and 3-bit coding metasurfaces are then designed using two different sets of reflection phases $\{0^\circ, 60^\circ, 120^\circ, 180^\circ\}$ and $\{0^\circ, 30^\circ, 60^\circ, 90^\circ, 120^\circ, 150^\circ, 180^\circ, 210^\circ\}$, respectively.

1. INTRODUCTION

Metasurfaces (MSs) consist of thin periodic and non-periodic sub-wavelength structures. This new class of artificial surfaces has attracted much attention due to its significant capability of manipulating electromagnetic waves. Numerous extraordinary functionalities have been introduced, such as the generalized law of reflection and refraction [1], perfect absorption [2], reflection/transmission phase modeling [3], polarization conversion [4], and holography [5]. Two major categories of metasurfaces were defined: static and dynamic. In the last few years, several researches and studies have focused on the development of dynamic programmable metasurfaces. In view of smart metasurfaces progress, dynamic coding metasurfaces [6] were proposed. Coding MSs is composed of N-types of units arrayed according to well-defined binary codes. Radar Cross Section reducing is one of the most favourable applications of coding metasurfaces. As a means to achieve this scattering field manipulation, the electromagnetic characterization of MS is a critical experience.

Hence, the design of metasurfaces has been studied massively based on the equivalent circuit model, effective impedance mode, FEM and FDTD methods [7–9]. However, in the case of coding metasurfaces, the design process becomes very challenging because their performance depends on many parameters such as physical propriety, geometry, the radiation pattern of each element, and the number of unit cells. In this context, the design of such metasurfaces [10, 11] should be considered as an optimization problem where the resolution tends to optimize the metasurface parameters in a desired manner. As reported in [12], beam rotation, resonance frequency shift, and radiation pattern reconfiguration of a monopole antenna have been studied and demonstrated using controllable metasurface. In fact, Ünüal and Altıntarla have used 1-bit coding metasurface based on digitally controlling the ON/OFF states using genetic algorithms. In this paper, based on graphene tunability, multi-bit coding metasurfaces are designed where the EM manipulation quality is improved by increasing the coding quantified levels.

Received 30 May 2018, Accepted 10 August 2019, Scheduled 26 August 2019

* Corresponding author: Imen Soltani (soltani.imen.enit@gmail.com).

The authors are with the University of Tunis El Manar, National Engineering School of Tunis, Sys'Com Laboratory, Tunis, Tunisia.

Here, the analysis of electromagnetic scattering from the graphene-based metasurface in the advantageous terahertz region is accomplished by the use of the MoM-GEC method. Furthermore, the GA is selected as an optimization tool to search the stochastic global layout of the MS, where the total scattering power is confined in a lower degree in all directions.

2. THE MOM-GEC METHOD

The method of moments presents the most sufficient and global method to study discontinuities and to reduce the problem of dimensions by writing its boundary conditions in the form of integral equations. However, the process of solving this type of integral equations is expensive in terms of memory and time consumption. As long as the computational sophistication deeply depends on the studied structure geometry and parameters. The introduction of the Generalized Equivalent Circuit's method (GEC) [13] presents the ultimate enhanced methodology to develop a simple integral equation formulation. The GEC method was proposed for the purpose of translating the electromagnetic resolution procedure (E, H) from the integral equations domain to the equivalent circuit's one (V, I). Thus, a systematic derivation process of integral equations based on the introduction of operators — connected to Green's operators with one fundamental function — instead of conventional impedance and admittance parameters is presented. Consequently, an electric image of the studied structure is created based on the discontinuity model. Accordingly, the EM discontinuity states are accurately described by trial functions. Therefore, the magnetic field (H) is substituted by the current density J_e defined as $J_e = \vec{H} \wedge \vec{n}$, where \vec{n} is the normal vector to the discontinuity plane. In addition, the modeling with GEC needs the presence of impedance or admittance operators, excitation sources, virtual sources, and an adequate waveguide walls choice for illustrating the physical problem.

2.1. Impedance and Admittance Operators

In the discontinuity plane, the boundary conditions are presented by a surface impedance \hat{Z} (or admittance \hat{Y}) operator as depicted in Figure 1. Using these operators, we can deduce the relation between the field and current on the surface by a simple equation.



Figure 1. Representation of the impedance operator.

2.2. Excitation Source

The located and modal sources are used to represent the excitation source at the discontinuity surface. This excitation source is called real source which delivers energy and can be either current or field source. The representation of real field and current sources is illustrated in Figure 2.

2.3. Virtual Source

The electromagnetic state of the discontinuity is described by generalized trial (test) functions. Those test functions are integrated in an equivalent circuit by a virtual source which does not deliver energy. The representation by virtual sources permits the expression of all passage relations imposed on electromagnetic field when traversing a discontinuity. Two types of test functions are used, where the current test function defines the graphene patterns, and the field test function represents the dielectric ones. These two representations are shown in Figure 3.

A suitable choice of test functions is of great interest to obtain the convergence of the solution, whereas their inadequate choice can complicate the problem or not solve it. Generally, a roughly high

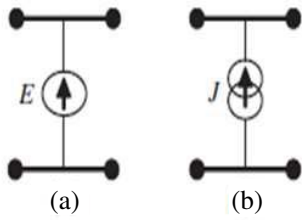


Figure 2. Symbolic notation of excitation sources: (a) Field excitation source; (b) Current excitation source.

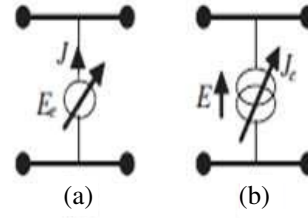


Figure 3. Symbolic notation of virtual sources: (a) Field source; (b) Current source.

number of sinusoidal and triangular test functions are used to get the solution. In this paper, we will use the sinusoidal test function.

3. APPLICATION OF MOM-GEC METHOD ON THE METASURFACE UNIT CELL

A MoM-GEC-based MATLAB code is used to perform the electromagnetic analysis of the MS' unit cell. As illustrated in Figure 4(a), the unit cell is immersed in a rectangular (EEEE) electric waveguide with 'a' and 'b' dimensions in *x-y* axis, respectively. Indeed, the front part of the waveguide is infinite (open-circuited) outlined in detail by an impedance operator \hat{Z}_M as depicted in Equation (1). Besides, the back part is short-circuited described by an admittance operator \hat{Y}_{sub} as shown in Equation (2). The two operators are written based on the modal basis of the waveguide, which are expressed by the waveguide modes $f_{m,n}$ [14, 15] and the total modal admittance and impedance for $TE_{m,n}$ and $TM_{m,n}$ modes: $z_{(mn,Top)}^{(TE,TM)}$ and $y_{(mn,Bottom)}^{(TE,TM)}$.

$$\hat{Z}_M = \sum \left| f_{m,n} \right\rangle z_{(mn,Top)}^{(TE,TM)} \left\langle f_{m,n} \right| \tag{1}$$

$$\hat{Y}_{sub} = \sum \left| f_{m,n} \right\rangle y_{(mn,Bottom)}^{(TE,TM)} \left\langle f_{m,n} \right| \tag{2}$$

The graphene ribbon is characterized by a surface impedance operator Z_s . In fact, Z_s is calculated using the graphene sheet surface impedance per unit length as highlighted in Equation (3), which can be defined as the sum of resistance R_s and reactance X_s .

$$Z_s = \frac{1}{\sigma(\omega)} = R_s + jX_s \tag{3}$$

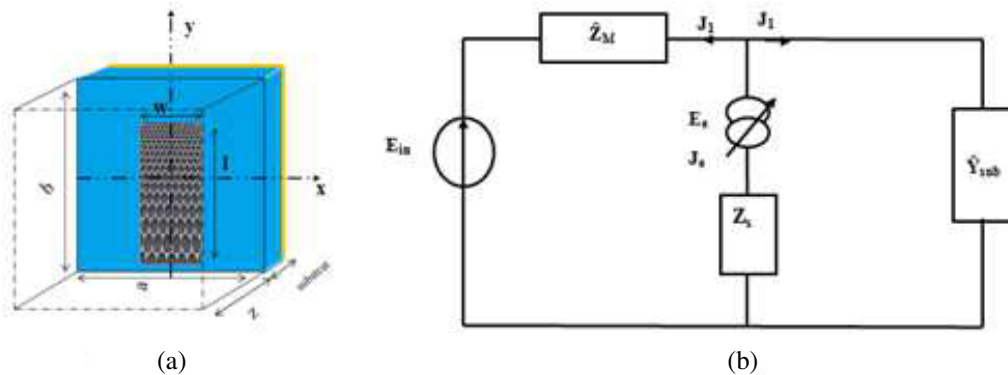


Figure 4. (a) The proposed MS unit cell, $l = 7.5 \mu\text{m}$, $w = 1.5 \mu\text{m}$, $a = b = 16 \mu\text{m}$ at frequency 2 THz. (b) The generalized equivalent circuit.

So, the parameter σ used in Equation (3) is the complex conductivity of graphene derived from Kubo formulation [16] as:

$$\sigma(\omega) = \frac{e^2}{\pi\hbar^2} \frac{2K_B T}{\tau_{eff}^{-1}(\omega)j\omega} \ln \left(2 \cosh \frac{E_f}{2K_B T} \right) \quad (4)$$

where E_f = chemical potential (ev), ω = Angular frequency, T = Temperature in units of K , K_B = Boltzmann constant, \hbar = Planck's constant, e = Electron volt, τ^{-1} = relaxation frequency.

The unit cell is excited by a TEM source E_{in} as illustrated in Figure 4(b). The resolution of this electromagnetic problem tends to calculate the current density J_e occurring on the graphene part. J_e can be expressed as:

$$J_e(x, y) = \sum_{i=1}^{N_y} x_i g_i(x, y) \quad (5)$$

where N_y is the number of trail (test) functions g_i .

Using the Kirchoff's and Ohm's laws applied to the equivalent circuit of Figure 4(b) leads to the following equation system:

$$\begin{cases} J_e = J_1 + J_2 = J_0 & (6a) \\ E_{in} - \hat{Z}_M J_1 + \hat{Z}_s J_e - E_e = 0 & (6b) \\ E_e - \hat{Z}_s J_e = \hat{Y}_{sub} J_2 & (6c) \end{cases}$$

The equation system (6) can be written in matrix form connecting the real source $E_{in}(= V_0 f_0)$ and virtual source E_e to these dual quantities. Current J_0 is defined as mode functions combination of basis function $f_{m,n}$: $J_0 = I_0 f_0$.

$$\begin{bmatrix} J_0 \\ E_e \end{bmatrix} = \begin{bmatrix} 0 & (\hat{Y}_{sub} \hat{Y}_M + 1) \\ -(\hat{Y}_{sub} \hat{Y}_M + 1) & \hat{Y}_{sub} + \hat{Y}_M + \hat{Z}_s \end{bmatrix} \begin{bmatrix} E_{in} \\ J_e \end{bmatrix} \quad (7)$$

By applying the Galerkin method, the EM problem is described by a matrix equation combining matrix 'B' of boundary conditions, matrix 'A' of the excitation term, and the unknown vector 'X' composed of x_i coefficient of current density J_e . In this sense, the matrix system in Eq. (7) will be conveyed as:

$$\begin{bmatrix} I_0 \\ [0] \end{bmatrix} = \begin{bmatrix} 0 & A \\ -A^T & B \end{bmatrix} \begin{bmatrix} V_0 \\ [X] \end{bmatrix} \quad (8)$$

where

$$B[i, j] = \langle g_i | \hat{Z}_M g_j \rangle + \langle g_i | \hat{Z}_s g_j \rangle + \langle g_i | \hat{Y}_{sub} g_j \rangle \quad (9a)$$

$$A[i] = V_0 \langle g_i | f_0 \rangle + V_0 \langle g_i | \hat{Y}_M \hat{Y}_{sub} f_0 \rangle \quad (9b)$$

Now, the input impedance and the reflection coefficient can be deduced as depicted in Equations (10) and (11), respectively.

$$Z_{in} = (AB^{-1}A^t)^{-1} \quad (10)$$

$$S_{11} = \frac{Z_{in} - Z_{TEM}}{Z_{in} + Z_{TEM}} \quad (11)$$

where $Z_{TEM} = 377 \Omega$.

A convergence study of our method is an important task applied to ensure the numerical results stability. As shown in Figure 5(a), we are able to calculate the input impedance Z_{in} at a stability condition (trail functions number $N_Y = 15$ and 140×140 modes (basis functions numbers)). Accordingly, the relationship between the reflective phase and chemical potential parameter E_f can be imitated by solving Equation (11) for different E_f as illustrated in Figure 5(b).

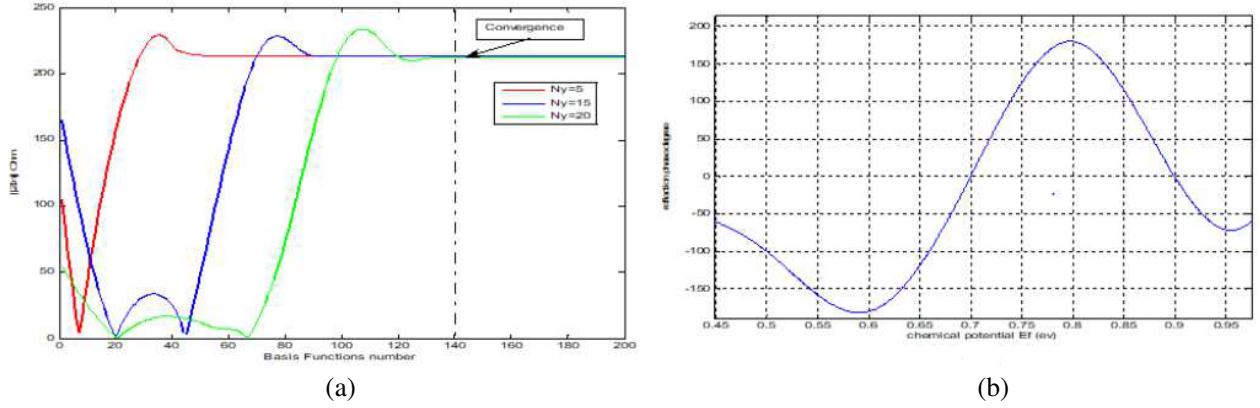


Figure 5. (a) MoM-GEC convergence and stability study. (b) Reflection phase evolution as a function of graphene chemical potential E_f .

4. METASURFACE DESIGN USING GENETIC ALGORITHMS

According to the coding metasurface design, a metasurface composed of $M \times N$ graphene based elements of varied reflection phases is proposed. Primarily, two coding elements owing to two opposite reflection phases “0°” and “180°” are generated by varying the chemical potential of the graphene ribbon E_f , for $E_f = 0.7$ eV and $E_f = 0.8$ eV, respectively. The reflection amplitude of each unit cell is normalized to 0.99 due to the gold film grounded in the back. Based on the antenna array theory [17], the total scattering field of the array can be expressed as:

$$TSF_{m,n}(\theta, \varphi, \varphi_r) = \sum_{m=1}^M \sum_{n=1}^N AF_{m,n}(\theta, \varphi, \varphi_r) * EP \tag{12}$$

φ, θ are the azimuthal and polar angles, respectively. $\varphi_r(m, n)$ is the reflection phase at each unit cell. EP represents the radiation pattern of each unit cell, is equal to 1 (isotropic), and will be neglected in our design. $AF_{m,n}(\theta, \varphi, \varphi_r)$ is the array factor expression as highlighted in Equation (13), where d_x and d_y are the distance between two adjacent elements along the x and y directions, respectively.

$$AF_{m,n}(\theta, \varphi, \varphi_r) = \sum_{m=1}^M \sum_{n=1}^N \exp(i\varphi_r(m, n)) \exp\left(i\frac{2\pi}{\lambda} \left(d_x \left(m - \frac{1}{2}\right) \sin \theta \sin \varphi + vd_y \left(n - \frac{1}{2}\right) \sin \theta \sin \varphi\right)\right) \tag{13}$$

To achieve the goal of reducing RCS, a real number encoding genetic algorithm is adopted to implement the optimal layout determination. The genetic algorithm is a global optimization algorithm that simulates the natural selection process. So, the GA approach is populated by selection, crossover and mutation operators. In fact, an initial population enters the main GA loop to search for the optimum solution of the defined problem. This loop is controlled by the fitness function and termination conditions. Thus, the GA is an effective global optimizer suitable for binary coding electromagnetic problems.

In this article, the genetic algorithm operates directly on a gene of the binary coding sequence of reflection phase matrix. Every gene is transformed to an individual using Equation (13). A number of individuals form a generation. At every generation, the corresponding scattering performances are evaluated by minimizing the cost function illustrated in Equation (14).

$$\text{Cost} = \max(TSF_{m,n}) \tag{14}$$

Figure 6 shows the flowchart of the proposed layout optimization method and the evolution plot of the cost functions minimization: $\max(TSF_{4,4})$ and $\max(TSF_{8,8})$. As a result, the maximum value of the scattering field can be reduced.

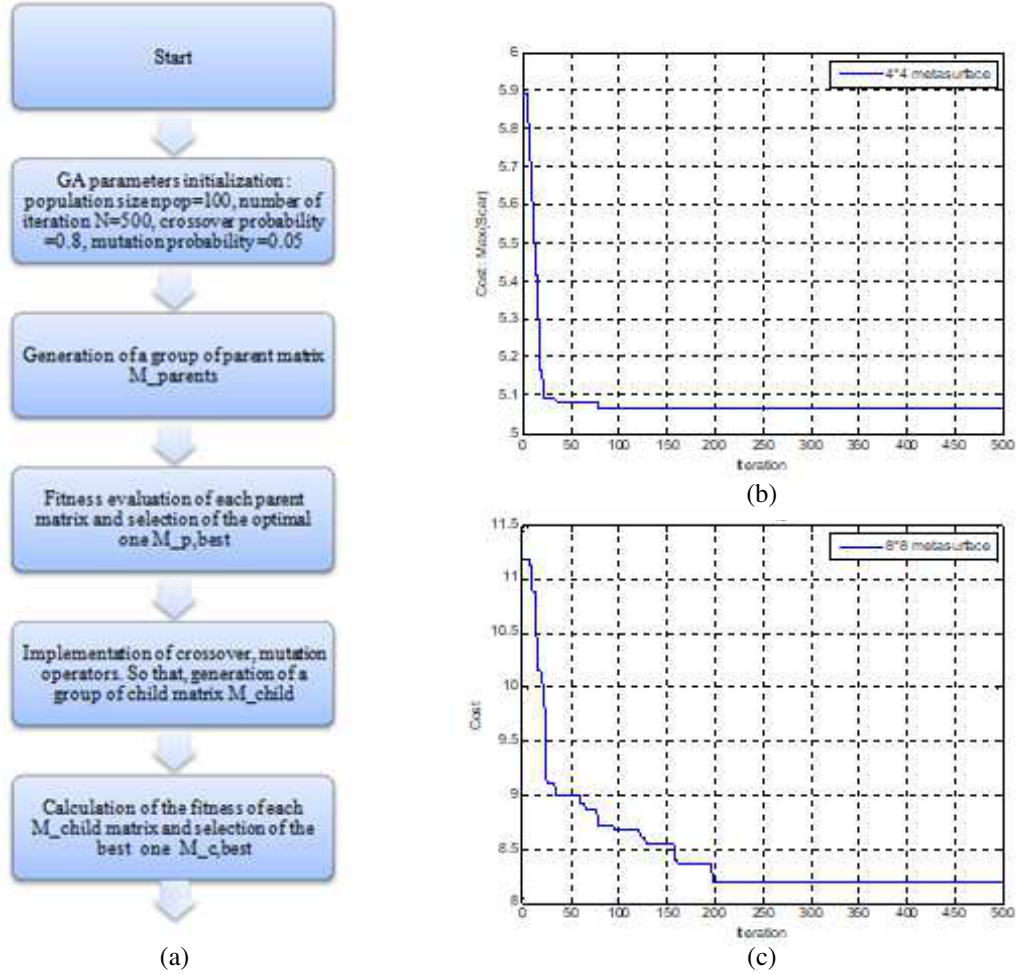


Figure 6. (a) GA flow chart. (b)–(c) The evolution plot of cost function reduction of $\max(TSF_{4,4})$, $\max(TSF_{8,8})$.

5. RESULTS AND DISCUSSION

In this section, metasurfaces of 8×8 , 16×16 , 32×32 , and 64×64 arrays under normal incidence have been designed and optimized using our modeling strategy. By comparing the array sizes, we are able to demonstrate that the RCS reduction increases when the unit cells number $N \times M$ is extended. 8×8 , 16×16 and 32×32 optimal coding phase distributions and their corresponding 2-D E -plane scattering fields are shown in Table 1.

Furthermore, the 2-D and 3-D scattering patterns of each optimized layout are depicted in Table 2. It can be clearly seen that the number of array elements directly affects the broadband scattering reduction. Thereby, with the growing amount of $N \times M$, the electric field scattering pattern of the optimized phase distributions shows that the diffusions are perfectly achieved. The diffusion effects of Terahertz waves are performed to 64×64 coding metasurfaces with 1-bit, 2-bit, and 3-bit coding sequences. It is clear that the energy is redistributed to multiple directions as illustrated in Figure 7.

The compartments of radar cross section reduction observed by 1-bit, 2-bit, and 3-bit metasurfaces are almost identical, but the diffusing of the electromagnetic waves of the 3-bit optimized coding layout is superior to the 1-bit and 2-bit metasurfaces responses.

Table 1. Summarizing table of 2D scattering field of each optimal metasurface.

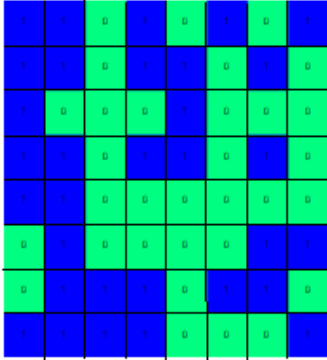
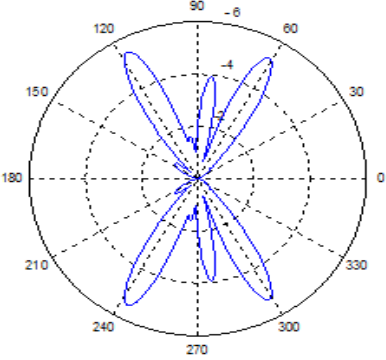
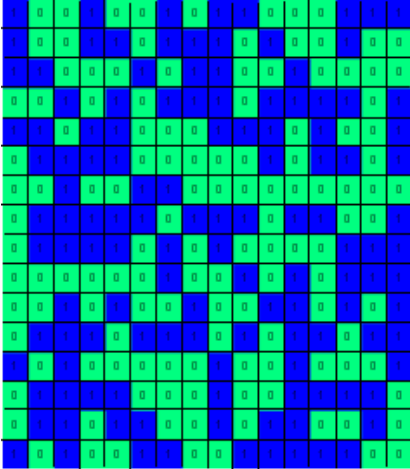
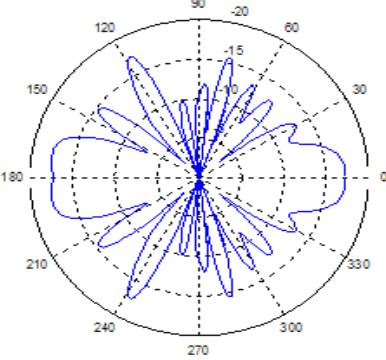
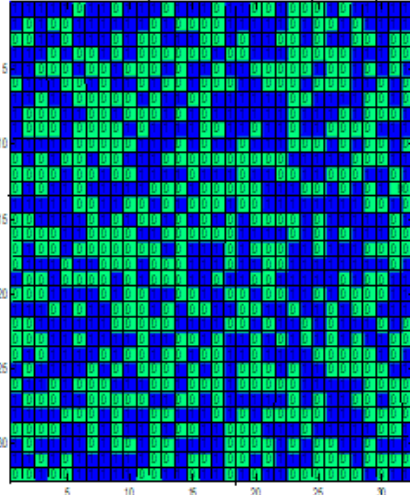
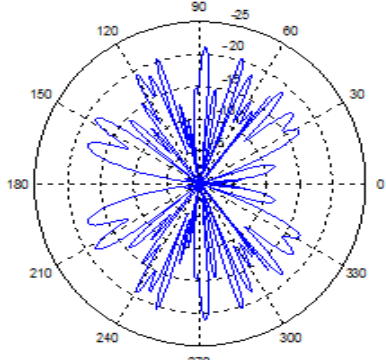
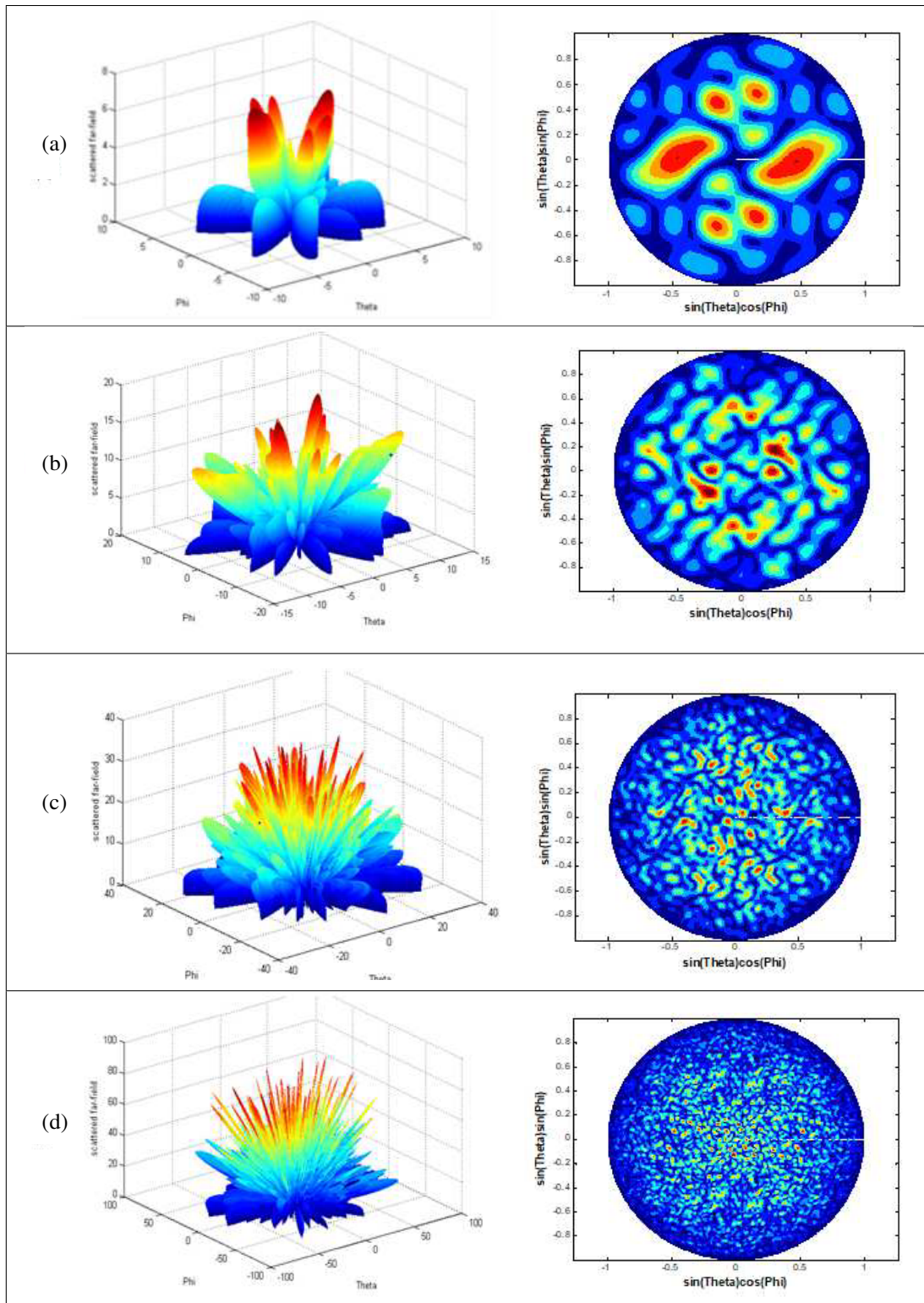
Array $M \times N$	Metasurface optimal layout	Scattering pattern (dBm)
8×8	 <p>An 8x8 grid of colored squares representing the optimal layout for an 8x8 array. The colors are blue and green, arranged in a complex, non-uniform pattern.</p>	 <p>Polar plot of the scattering pattern for an 8x8 array. The plot shows a central peak with several lobes extending outwards. The radial axis represents dBm, with values -6, -4, and -2. The angular axis represents degrees, with labels from 0 to 330 in increments of 30.</p>
16×16	 <p>A 16x16 grid of colored squares representing the optimal layout for a 16x16 array. The colors are blue and green, arranged in a complex, non-uniform pattern.</p>	 <p>Polar plot of the scattering pattern for a 16x16 array. The plot shows a central peak with several lobes extending outwards. The radial axis represents dBm, with values -20 and -15. The angular axis represents degrees, with labels from 0 to 330 in increments of 30.</p>
32×32	 <p>A 32x32 grid of colored squares representing the optimal layout for a 32x32 array. The colors are blue and green, arranged in a complex, non-uniform pattern. The grid is labeled with row numbers 5, 10, 15, 20, 25, 30 on the left and column numbers 5, 10, 15, 20, 25, 30 on the bottom.</p>	 <p>Polar plot of the scattering pattern for a 32x32 array. The plot shows a central peak with several lobes extending outwards. The radial axis represents dBm, with values -25 and -20. The angular axis represents degrees, with labels from 0 to 330 in increments of 30.</p>

Table 2. 2D and 3D scattering patterns of optimal 1-bit coding metasurfaces for different array numbers: (a) 8×8 ; (b) 16×16 ; (c) 32×32 ; (d) 64×64 elements.



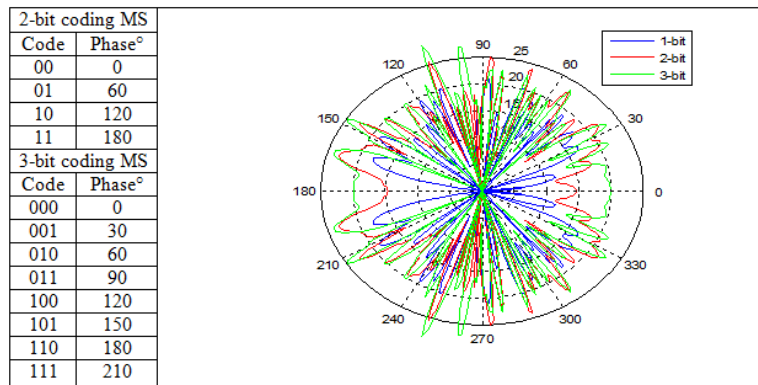


Figure 7. 2-D E -plane scattering fields of 64×64 coding metasurfaces with 1-bit, 2-bit and 3-bit coding sequences.

6. CONCLUSION

A multi-bit low RCS coding metasurface has been proposed. An isotropic graphene-based unit cell is modeled using the method of moments combined with the generalized equivalent circuit approach. In addition, to avoid strong energy appearing, the genetic algorithm is adopted to search the optimal reflection phase matrix and the layout of multiple elements metasurfaces. The results of optimal metasurfaces are in good agreement with the desired field diffusion characteristics. The 64×64 metasurface with 3-bit coding sequence presents the optimal desired performance.

REFERENCES

1. Achouri, K. and C. Caloz, "Space-wave routing via surface waves using a metasurface system," *Sci. Rep.*, Vol. 8, No. 1, 1–9, 2018.
2. Zhu, W., F. Xiao, M. Kang, and M. Premaratne, "Coherent perfect absorption in an all-dielectric metasurface," *Appl. Phys. Lett.*, Vol. 108, No. 12, 1–5, 2016.
3. Wu, K., P. Coquet, Q. J. Wang, and P. Genevet, "Modelling of free-form conformal metasurfaces," *Nat. Commun.*, Vol. 9, No. 1, 1–8, 2018.
4. Akgol, O., E. Ünal, O. Altintas, M. Karaaslan, F. Karadag, and C. Sabah, "Design of metasurface polarization converter from linearly polarized signal to circularly polarized signal," *Optik*, Vol. 161, No. 10 1968, 12–19, 2018.
5. Deng, Z.-L. and G. Li, "Metasurface optical holography," *Mater. Today Phys.*, Vol. 3, No. 5 9 2011, 16–32, 2017.
6. Jafar-Zanjani, S., S. Inampudi, and H. Mosallaei, "Adaptive genetic algorithm for optical metasurfaces design," *Sci. Rep.*, Vol. 8, No. 1, 1–16, 2018.
7. Nye, N. S., A. Swisher, C. Bungay, et al., "Design of broadband anti-reflective metasurfaces based on an effective medium approach," *Proc. SPIE 10181, Advanced Optics for Defense Applications: UV through LWIR II*, 101810J, Anaheim, California, United States, 2017.
8. Pulido-Mancera, L., P. T. Bowen, M. F. Imani, et al., "Polarizability extraction of complementary metamaterial elements in waveguides for aperture modeling," *Phys. Rev. B*, Vol. 96, No. 235402, 1–14, 2017.
9. Wu, K., P. Coquet, Q. J. Wang, et al., "Modelling of free-form conformal metasurfaces," *Nat. Commun.*, Vol. 9, No. 3494, 1–8, 2018.
10. Cui, T. J., M. Q. Qi, X. Wan, J. Zhao, Q. Cheng, K. T. Lee, J. Y. Lee, S. Seo, L. J. Guo, Z. Zhang, Z. You, and D. Chu, "Coding metamaterials, digital metamaterials and programmable metamaterials," *Light Sci. Appl.*, Vol. 3, No. 10, 1–9, 2014.

11. Feng, Y., K. Chen, B. Zhu, J. Zhao, T. Jiang, and L. Cui, "Coding metasurface for broadband microwave scattering reduction with optical transparency," *Opt. Express.*, Vol. 25, No. 5, 5571–5579, 2017.
12. Ünal, E. and G. Altıntarla, "Smart monopole antenna with pattern and frequency reconfiguration characteristics based on programmable metasurface," *Int. J. RF Microw. Comput. Eng.*, e21805, 2019.
13. Baudrand, H. and D. Bajon, "Equivalent circuit representation for integral formulations of electromagnetic problems," *Int. J. Numer Model Electron Networks, Devices Fields*, Vol. 15, No. 1, 23–57, 2002.
14. Hajji, M., M. Aidi, H. Krraoui, and T. Aguilí, "Hybridization of generalized Po and Mom-Gec method for electromagnetic study of complex structures: Application to reflectarrays," *Progress In Electromagnetics Research M*, Vol. 45, 35–49, 2016.
15. Aidi, M., M. Hajji, B. Hamdi, and T. Aguilí, "Graphene nanoribbon modeling based on MoM-GEC method for antenna applications in the terahertz range," *2015 World Symposium on Mechatronics Engineering and Applied Physics (WSMEAP)*, No. 2, 1–4, Sousse, 2015.
16. Ziegler, K., "Robust transport properties in graphene," *Phys. Rev. Lett.*, Vol. 97, No. 26, 1–5, 2006.
17. Balanis, C. A., *Antenna Theory: Analysis and Design*, 4th Edition, John Wiley and Sons, Inc., New York, NY, USA, 2016.